Anomalous enhanced emission from PbS quantum dots on a photonic-crystal microcavity

Ting Shan Luk,[1,2,*] Shisheng Xiong,[3] Weng W. Chow,[2,4] Xiaoyu Miao,[5] Ganapathi Subramania,[2] Paul J. Resnick,[2] Arthur J. Fischer,[2] and Jeffrey C. Brinker[2,3]

[1]*Center for Integrated NanoTechnologies, Sandia National Laboratories, Albuquerque, New Mexico 87123, USA*
[2]*Sandia National Laboratories, Albuquerque, New Mexico 87185-1086, USA*
[3]*Center for MicroEngineered Materials, Department of Chemical and Nuclear Engineering, University of New Mexico, Albuquerque, New Mexico 87106, USA*
[4]*Physics Department and Institute of Quantum Studies, Texas A&M University, College Station, Texas 77843, USA*
[5]*Google Inc., 1600 Amphitheatre Parkway, Mountain View, California 94043, USA*
**Corresponding author: tsluk@sandia.gov*

Received February 15, 2011; accepted March 23, 2011;
posted April 7, 2011 (Doc. ID 142653); published May 9, 2011

We report up to 75 times enhancement in emission from lithographically produced photonic crystals with post-processing close-packed colloidal quantum-dot incorporation. In our analysis, we use the emission from a close-packed free-standing film as a reference. After discounting the angular redistribution effect, our analysis shows that the observed enhancement is larger than the combined effects of Purcell enhancement and dielectric enhancement with the microscopic local field. The additional enhancement mechanisms, which are consistent with all our observations, are thought to be spectral diffusion mediated by phonons and local polarization fluctuations that allow off-resonant excitons to emit at the cavity wavelengths.

OCIS codes: 230.0230, 140.3945, 350.4238, 300.2140.

1. INTRODUCTION

Quantum-dot (QD) emission in a microcavity has been intensively investigated recently due to rapid advances in achieving simultaneously high Q and small mode volume cavities [1]. Semiconductor QD emitters in microcavities have the potential to realize practical devices such as zero threshold lasers [2] and single and entangled photon sources [3,4], as well as advances in quantum optics research [5–8]. In addition, the ability to enhance the emission rate by photonic density of states control [9] is also important to silicon photonics [10], solid-state lighting [11,12], and solar cell applications [12,13].

In the case of good emitters, such as InAs QDs at low temperatures, in which the total dephasing and the radiative linewidth are both much smaller than the cavity linewidth, large enhancement in spontaneous emission have been clearly demonstrated in the weak coupling regime [14–16]. Recently, strong coupling behavior has also been demonstrated [17–19]. However, current understanding of nonideal or "bad emitter" systems in which the dephasing width is much larger than the radiative width and the cavity linewidth, is less clear [20–26]. Examples of bad emitters are colloidal infrared PbS and PbSe QDs, Si nanocrystals, and Er^{3+} ions in SiO_2 or silicon nitride. According to several theoretical studies [27–29], for emitter systems like PbS and PbSe QDs, the Purcell enhancement is negligible and is independent of the cavity Q factor but, rather, is determined by the emitter Q factor. Experimentally reported enhancement factors from "bad emitters" have a large amount of variation. A Purcell enhancement factor of 30 was reported by spin coating colloidal PbS QDs embedded in polymethyl methacrylate on a photonic-crystal microcavity with $Q = 400$ [20]. An enhancement factor of 10 has also been reported with a cavity Q of 3000 [24] using selective chemical adsorption activated by atomic force microscope (AFM) nanopatterning. In another case, PbS QDs attached to the cavity by soaking yielded an enhancement factor of 35 from a cavity with $Q = 775$ [22]. For Er^{3+} ions in silicon nitride, a room temperature enhancement factor of 1.4 was reported from a cavity with $Q = 6000$ [30]. None of these studies has demonstrated a linear dependence of enhancement factor to Q factor. In these PbS studies, the reported enhancement factor mechanism was attributed to the Purcell effect. In addition, for all these studies except for the AFM patterning case, the emitters are randomly distributed within the film and, therefore, the emitter distances from the surface of the photonic crystal are not well defined.

In this study, we measure the enhanced emission from PbS QDs with well-controlled dot-cavity locations with respect to a free-standing monolayer of close-packed QDs, which enables a stable reference with known angular distribution. A 20–50 nm thick polymer film supporting a monolayer of close-packed PbS QDs can be deposited onto the surface of a photonic-crystal microcavity where these QDs are located at the interface between the polymer and the photonic-crystal [31]. In this case, the surface of the cavity is uniformly covered with QDs and, therefore, there are an equal number of dots on the node and antinode regions of the cavity. The highest Q factor achieved with this technique is greater than 8000. After studying a large number of cavity-emitter structures, our measurements show no clear linear relationship between the enhancement factor and the cavity Q, suggesting that the enhancement mechanism is not dominated by the Purcell effect. Furthermore, we observe an enhancement factor larger than expected for the combined effects of Purcell, dielectric, and local field enhancements. We will present our experimental

results and discuss possible enhancement mechanisms that could play a role for QDs in a microcavity.

2. FABRICATION OF PHOTONIC CRYSTALS AND CLOSE-PACKED MONOLAYER POLYMER FILMS

For photonic-crystal and microcavity fabrication, the starting material is a 150 mm diameter silicon-on-insulator (SOI) wafer with a 250 nm thick silicon device layer with a $3\,\mu$m thick buried-oxide (BOx) layer. The pattern is a triangular lattice with lattice constant in the Γ-K direction of $a = 415$ nm and a hole diameter of 240 nm. A cavity is created in the photonic-crystal lattice by three missing air holes (L3) as shown in Figs. 1(a)–1(c). The cavity has the end-hole positions shifted away from the cavity by nominal values of $0.18a$, $0.025a$, and $0.18a$, as in the design by Akahane *et al.* [32]. Devices fabricated thereby have 100–300 holes in the Γ–K direction with a waveguide along this direction and 15 holes in the Γ–X direction. We use commercially available, mass-production semiconductor processing tools throughout the fabrication process. A waveguide is also fabricated that can be used to couple an external source into the microcavity. The coupling strength is controlled by the number of holes between the waveguide and the cavity. In particular, we will discuss results associated with the $1.0W_1$ waveguide defect, which is a row of missing holes.

All lithography was performed on an ASML PAS 5500 Step-and-Scan system, and all dry etching was performed with an Applied Materials Centura platform tool. The first lithographic layer defines the photonic crystal by patterning the 240 nm diameter holes in the photoresist. This pattern is transferred into the device layer using reactive ion etching (RIE), optimized for straight vertical sidewalls. A second mask level was used to etch the substrate on either side of the device for optical access. A deep RIE (DRIE) process was used to create roughly $80\,\mu$m deep grooves into the silicon to provide optical coupling of the lensed fiber to the waveguides. To protect the photonic crystal that had been etched into the device layer, an 850 nm polysilicon film was deposited on top of a $2\,\mu$m thick oxide film and then patterned with a photoresist mask. The polysilicon hard mask was used for the oxide etch steps because relatively thick oxide films were employed ($2\,\mu$m hard mask, $3\,\mu$m BOx). The oxide film served as a hard mask for the DRIE Si etch. During the BOx etch, the photoresist mask is consumed and the polysilicon hard mask is used to define the pattern. During the DRIE handle etch, the polysilicon mask is also consumed so that the underlying $2\,\mu$m oxide film now acts as the mask to protect the silicon photonic-crystal device. Finally, hydrofluoric acid was used to strip the remaining oxide hard mask, as well as to undercut the SOI BOx below the lattice. A timed etch was used so that the oxide was stripped below the lattice to produce an air-clad photonic crystal, but sufficient oxide remained at the edge of the device to anchor the structure to the substrate. Figure 1(a) shows scanning electron microscope (SEM) images of a fabricated photonic-crystal device.

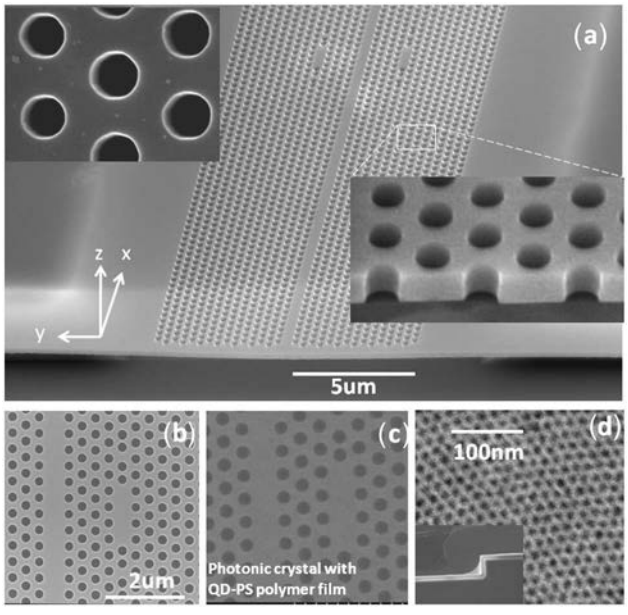

Fig. 1. (a) SEM image of a two-dimensional silicon membrane photonic-crystal device consisting of two L3 cavities and a waveguide supported with SiO_2 anchors. The top left inset shows the top view of the holes on the silicon membrane. The lower right inset shows the sidewall profile of the holes. (b) Top SEM view of the L3 cavity created by three missing air holes. (c) SEM image of a cavity with polymer film on top. (d) TEM image of a monolayer of PbS in P3HT polymer. Lower left inset shows a free-film hanging by a corner feature of the photonic-crystal sample.

A monolayer of close-packed PbS QDs (purchased from Evident Technologies) was created using evaporation-induced nanoparticles/polymer self-assembly [33] at a fluid interface, followed by monolayer transfer, as was recently reported [31]. Because the monolayer has a high modulus, it remains suspended over air holes without adhering to the side walls. A suspended film with a sufficiently large area is also present in certain parts of the chip to enable free-film photoluminescence (PL) measurement, which is used as a reference signal. A transmission electron microscope (TEM) image of the QD film transferred onto a holey carbon grid is shown in the inset of Fig. 1(d). The close packing gives a QD density of $10^4\,\mu\text{m}^{-2}$, which is over 2 orders of magnitude higher than that of the typical Stranski–Krastanov growth method. The density and uniformity are sufficiently high to relax the requirement of matching QD locations to the antinode region of the cavity mode. Moreover, colloidal QDs provide greater integration flexibility with photonic crystals and nanostructured photonic materials. Using this approach, incorporation of QDs occurs during postprocessing, under ambient conditions using self-assembly of ligand functionalized QDs [24,33,34].

To measure the PL of the excited QDs, we used a standard micro-PL setup where the excitation source and PL signal are focused and collected through a 0.65 NA Mitutoyo 50× NIR HR microscope objective. This objective has a collection efficiency of 42% of the upper hemisphere. The field of view of the detection optics has about a $15\,\mu$m diameter. The excitation source is a cw 830 or 904 nm diode laser delivered by a single-mode $5.6\,\mu$m core fiber collimated to match the entrance pupil of the objective. We have not noticed any significant difference in the enhancement factor when switching between these two laser sources. However, the 904 nm laser appears to have a smaller photobleaching effect. A diffraction-limited spot size of $1.6\,\mu$m $1/e^2$ diameter is produced on the sample in the presence of a $175\,\mu$m thick coverslip. The out-of-plane PL is collected by the same objective and coupled to a

0.3 or 0.5 m imaging spectrometer through a 50 μm diameter multimode fiber capable of achieving a spectral resolution of 0.4 and 0.1 nm, respectively. An OMAV InGaAs array detector is used to detect spectrally dispersed emission.

3. OPTICAL MEASUREMENTS

A. Spectroscopy of Microcavity Resonances

Emission comes mostly from the radiative recombination of ground electron and hole states, involving states populated via collisional relaxation from higher lying levels on a picosecond time scale [35]. The fact that the PL signal has no dependence on the excitation polarization is consistent with this pump relaxation process [36]. However, the PL from the cavity resonance is highly polarized and is present only when the QDs on the cavity are excited. The wavelengths of the resonances are expected to be slightly different from sample to sample due to variation in the polymer film thickness, but their relative positions are very reproducible and in agreement with finite-difference time-domain (FDTD) calculations. We have used both poly-3-hexylthiophene (P3HT) and polystyrene (PS) polymers for the deposition and the difference in performance turned out to be relatively minor. A typical emission spectrum is shown in Fig. 2. The highest Q factor observed is from the E_y3 resonance with a Q factor greater than 8000 using PS as the polymer matrix material. The broad background emission is from QDs that are either not coupled to the cavity or are outside the cavity region excited by the laser. This broad background emission is very similar to the one obtained from a free-standing film (free-film). The weak feature at 1560 nm for the E_x polarization is the $1.1W_1$ waveguide mode probably excited due to imperfect placement of the excitation spot. The other small features on the short wavelength side of the E_x1 resonance are hybridized modes caused by the coupling between the waveguide and the cavity.

For calculations of the photonic-crystal band structure, wavelengths of microcavity resonances, and Q factors, we use the MIT Electromagnetic Equation Propagation simulation environment [37]. The photonic-crystal structure including the polymer film is discretized into a three dimensional computational supercell of $20 \times 16 \times 20$ periods. QD emission is simulated by an arrangement of multiple point current sources covering the waveguide and L3 cavity. For each point source, we use a Gaussian pulse centered at a reduced frequency of 0.273 (in unit of $c/2\pi a$) with a frequency spread of 0.05. Computation of the resonant frequencies together with their quality factors (Q) were performed with the harmonic inversion technique [38]. Unlike the more commonly used Fourier transform, harmonic inversion describes the signal using an adaptive, finite length series of decaying and nondecaying sinusoids. The respective time series of the electric components for use with harmonic inversion were detected in the far field at 8 periods (computational unit cells) away from the sources. For the modal field calculations, we use a narrower (than QD emission) bandwidth for the point sources and tune the emission frequency around the neighborhood of the mode resonances. The modal patterns for E_x1, E_y2, and E_y3 are shown in Fig. 2. The quantitative agreement between theory and experiment is to within 1.5% in the resonant frequencies, as summarized in Table 1. For the E_x1 resonance, the measured Q factor is consistently higher than the calculated value. This may be due to the sensitivity of the cavity geometry; a very slight difference between input and actual cavity parameters may result in noticeable discrepancies. Examples of sensitive parameters include side-wall straightness and hole locations and diameters [32]. In addition, the integrated PL signal from the cavity-free patterned region is comparable to that obtained from a free-film, indicating that

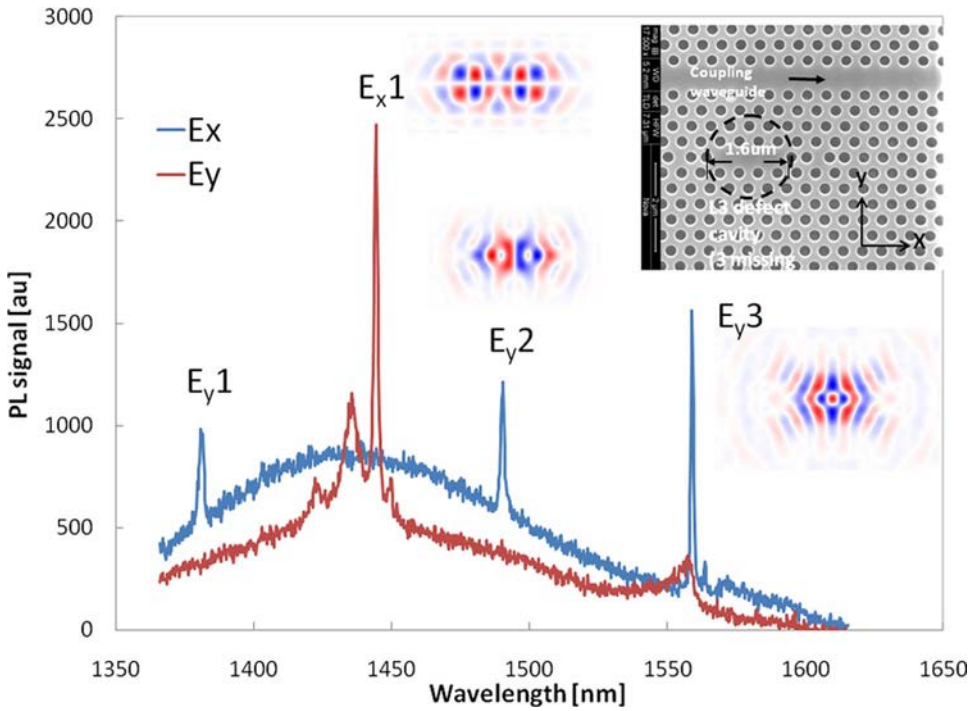

Fig. 2. (Color online) Measured photoluminescence (PL) spectrum taken from the same L3 cavity with polarization parallel (E_x) and perpendicular (E_y) to the long axis of the cavity. The calculated modal patterns are shown next to resonance peaks. The inset shows the excitation spot size relative to the cavity.

Table 1. Calculated and Measured Wavelengths and Q Factors of Cavity Resonances[a]

$\omega a/2\pi c$	Identification	λ (expt/cal)	Q_{max} (expt/cal)	Experimental Uncertainty (nm)
E × WG	E_x1	1457.9/1455.04	600/416	+/ – 3
E//WG	E_y1	1399/1396	720/1214	+/ – 10
E//WG	E_y2	1512.44/1511.7	1257/2182	+/ – 11
E//WG	E_y3	1580.74/1582.7	8028/16108	+/ – 9

[a]E//WG means the electric field polarization of the PL is parallel to the waveguide (WG) and E × WG means the polarization of the PL is perpendicular to the WG.

the PL signal is not being trapped or scattered outside the field of view of the detection system.

B. Angular Distribution Measurements

In order to be able to determine the enhancement factor of the emission, it is necessary to normalize the cavity-resonance emission to the emission in the absence of cavity influences. We chose emission from a free-film as the reference because (1) the angular distribution from the film is guaranteed to obey the cosine law and (2) the PL intensity is very stable and uniform to within 20%. While the emission from the cavity-free patterned region is typically used as a reference in other work [21], we find this to be less reliable since the angular distribution is not necessarily a cosine law distribution and it can be affected by any buckling of the photonic-crystal membrane structure. The angular distributions of the free-film and cavity-free pattern region are shown in Fig. 3. Although the two distributions are somewhat similar, the uncertainty for the lattice emission is significantly larger. We have also found that the intensity from the cavity-free pattern region depends on the conformity of the film to the photonic-crystal surface.

The high resolution angular distribution of the cavity emission is difficult to measure because a large numerical aperture objective is needed to collect sufficient luminescence signal from the cavity. A coarse measure of the angular behaviors and collection efficiencies of the cavity resonances is possible using different numerical aperture focusing/collection objectives (shown in Fig. 4). The PL signals from 20× and 10× objectives are normalized to the collection efficiency value of 0.42 of the 50× objective assuming a Lambertian source. To ensure this methodology is correct, we use the emission from a free-film as a test case and obtained the expected Lambertian behavior. From these measurements, we determined that the emission from the free-film and anchor (pattern-free) regions have very similar behavior. Both E_x1 and E_y2 resonances do not have their emission intensity peaked toward the normal direction due to significantly weaker signal than the cosine law distribution when the 10× objective was used. These behaviors are consistent with the angular distributions obtained from numerical simulations shown in the insets of Figs. 4(c) and 4(d). The key conclusion from these measurements is that none of these emissions has a very directional behavior, which can render gross errors in the enhancement factor estimates, which will be discussed in Subsections 3.C and 3.D.

C. Enhanced Emission from the Fabry–Perot-Like Waveguide Resonances

Along the y direction, the waveguide can be viewed as a Fabry–Perot (FP) cavity bounded by two photonic lattice mirrors. The propagation vector of the FP cavity modes is along the y direction and, therefore, its electric field is along the x direction. This identification is consistent with the observed redshift of 10% of the resonance wavelength when the waveguide width is $1.1W_1$ instead of $1.0W_1$. When the excitation source is focused on the waveguide, enhanced emission along x polarization is observed, as shown in Fig. 5. This emission is 5–8 times larger than that of the free-film. The background emission arises from the emitters not coupled to either the FP cavity resonance or to the photonic-crystal slab that emit into free space outside the sample. The excitation area is defined by the excitation spot diameter along the x direction and the width of the waveguide in the y direction; therefore, this area is comparable to the L3 microcavity. Correcting for excitation area that can couple to the waveguide (area ratio = 6), the emission rate is approximately 30–48 times larger than for a free-film even if

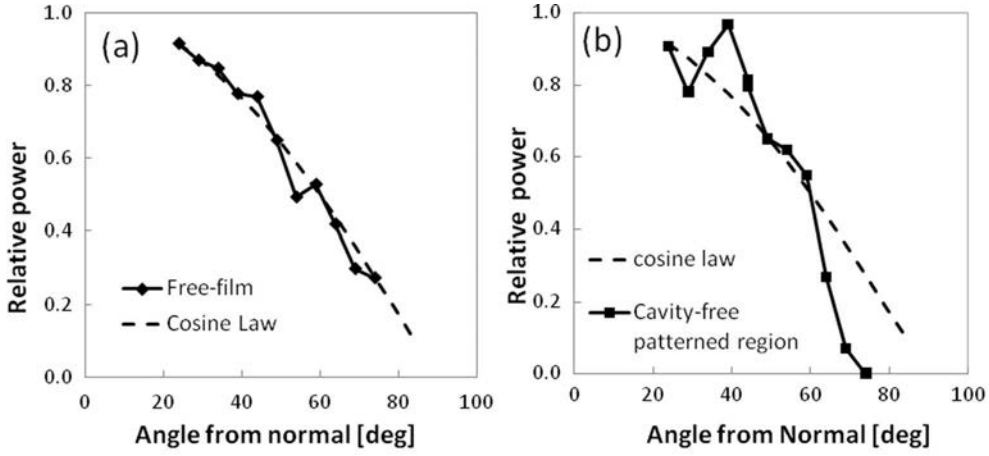

Fig. 3. Measured angular distribution of photoluminescence from (a) a free-film and (b) a cavity-free patterned region with a monolayer of close-packed QDs. All data are normalized to the value of cos(24°), which is the smallest angle the apparatus can measure.

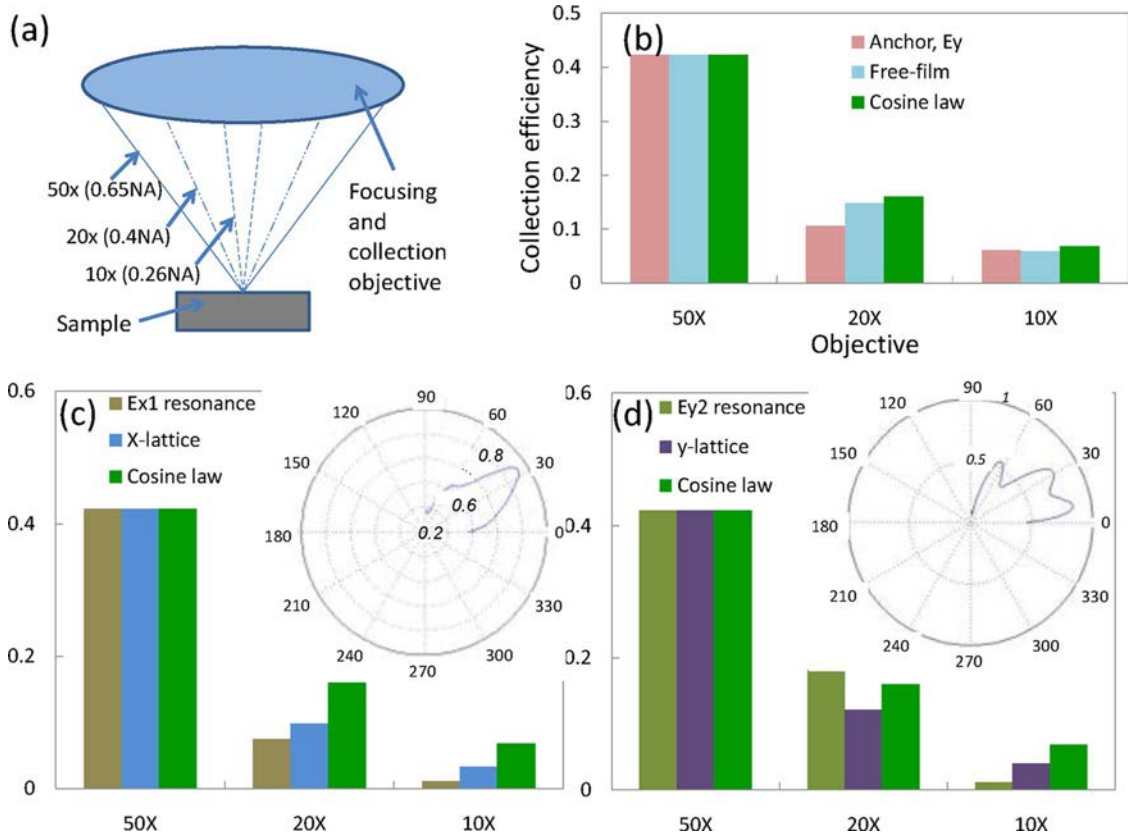

Fig. 4. (Color online) (a) Schematic drawing depicts the collection geometries of different numerical aperture (NA) objectives. The relative collection efficiency of the PL signals from 20× and 10× objectives are normalized to the Lambertian collection efficiency valued 0.42 for 50× objective. (b) The relative collection efficiency behaviors of the PL from free-film, the anchor region, and the cosine law show minor deviation from the cosine law behavior. The relative collection efficiencies of (c) E_x1 and (d) E_y2 resonances using a 10× objective are much smaller than cosine law behavior, indicating the emission is directed away from normal in agreement with simulation results (insets).

one assumes a 100% collection efficiency [39]. No such distinct resonance from any waveguide is observed in the y polarization.

As mentioned before, the Purcell effect is small because of the low emitter Q. However, the dielectric enhancement mechanism does not depend on the Q factor of the emitter or the cavity Q. It is known that the presence of high refractive index material enhances the emission rate by a factor of n in a conventional macroscopic field correction [40]. This arises from the fact that the vacuum field amplitude is reduced by a factor of n, but the free-space density of states increases as n^3. However, this enhancement mechanism does not include the local field effect. It was pointed out [41–43] that the local field effect can introduce a significant correction to the macroscopic picture as the spontaneous emission rate of a dipole in a dielectric medium is given as $\Gamma_D = (nL^2)\Gamma_{\text{vac}}$, where Γ_D and Γ_{vac} are the decay rates of an emitter in a dielectric and vacuum, respectively, and L is the local field enhancement factor. There are many local field models: for the real-cavity model, $L = (3n^2)/(2n^2+2)$ [44]; for the virtual cavity, $L = (n^2+2)/3$ [42,45]; and from the Crenshaw model [41,46], $L = ((n^2+2)/3n)^{1/2}$. These enhancement factors are shown in Fig. 6. Experimental studies [42,47] in the index range of 1.3–1.7 have shown good agreement with the real-cavity model. Based on the real-cavity model for silicon, a significant dielectric enhancement factor $\text{EF}_D = nL^2 = 7.3$ is obtained.

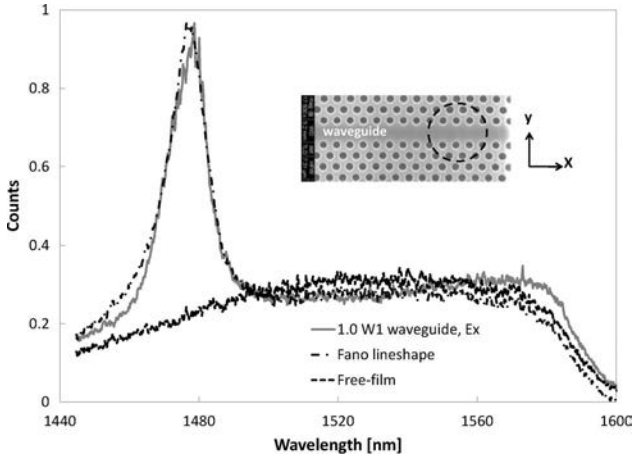

Fig. 5. Enhanced E_x emission from the FP-like resonance of the $1.0W_1$ waveguide (solid curve), free-film (dashed curve) and the Fano profile fit (dashed–dotted curve). Subtracting the peak signal from the background, the integrated signal corrected for the mode area in the peak is 85% of the total spectrally integrated free-film emission to the upper hemisphere. The inset shows the excitation region and the polarization direction.

We determined the dielectric enhancement factor for the free-film on a TEM grid to be 1.8 by comparing the emission of a free QD/polymer film. Since the QDs reside on the polymer–air interface, their emission into the polymer side is enhanced compared to the other side. This measurement provides an independent confirmation that the film is indeed thin enough that there are no trapped modes that could render a poor choice of reference. The measured value is slightly

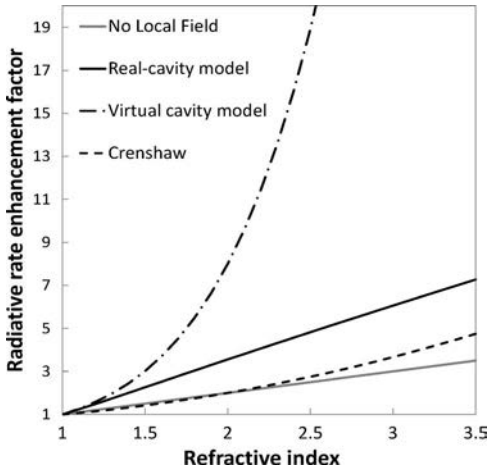

Fig. 6. Combined enhancement from dielectric and from different localized field models.

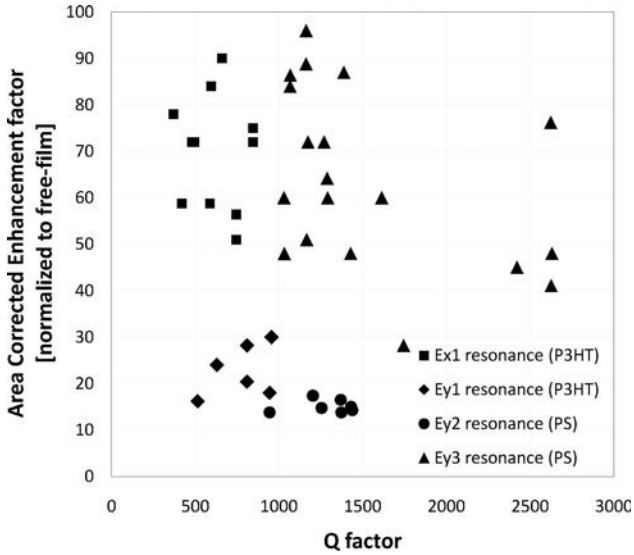

Fig. 7. Measured enhancement factor of E_x1, E_y1, E_y2, and E_y3 microcavity resonances with respect to the free-film. The enhancement factor is determined by the height of the resonance above the background emission divided by the emission of a free-film at the resonant frequency. The effect of excitation area to the cavity area is not included. Determination of the enhancement factors from higher Q cavities are unreliable due to poor signal-to-noise ratio of the reference signal since a higher resolution grating was required.

smaller than the expected 2.26 based on the real-cavity model. We believe this is due to the mean field effect because the film thickness is much smaller than the emission wavelength.

To determine the expected enhancement factor, we include the effects of the emitter area (A), enhanced absorption factor (E_A), dielectric enhancement (EF_D), Purcell cavity effect enhancement ($\mathrm{EF}_{\mathrm{cav}}$), coupling strength to the photonic-crystal cavity (β), coupling strength to free space from the cavity (η_{FS}), and collection efficiency (η_C). Therefore, we write the expected signal (S) as $S = A \cdot E_A \cdot \mathrm{EF}_D \cdot \mathrm{EF}_{\mathrm{cav}} \cdot \beta \cdot \eta_{\mathrm{FS}} \cdot \eta_C$, and the values in this expression for the free-film, waveguide, and E_x1 resonances are shown in Table 2.

An enhanced absorption factor $E_A = 1.3$ takes into account that the QDs residing on the surface of Si experience another pass of the excitation beam because the reflectivity of silicon is about 30%. This value is consistent with the increase in the background signal from a cavity-free patterned region, as shown in Fig. 6. In addition, we have performed FDTD simulation to ensure there is no accidental enhancement due to surface mode or guided modes in the upper band of the photonic-crystal lattice [48]. We assign the coupling efficiency from cavity to free space η_{FS} to 1 based on the numerical simulation studies of the dipole emitter in a general microcavity [49,50]. For the collection efficiency η_C, we assign the value of 1 to obtain the maximum enhancement effect from angular redistribution. A value less than 1 would result in a larger net enhancement effect. Together, the observed enhancement factor is still approximately 5 times below what we observed. It is worth noting that the amount of energy per unit area within the FP-like resonance peak is 85% of that emitted by the free-film into a 2π solid angle. This modified emission can be viewed as an act of spectral compression by the resonant cavity that directs the emission of QDs to the resonant wavelength. More discussion of this mechanism is in Section 4.

D. Enhanced Emission from Microcavities

As discussed in Section 1, we use free-film emission as the reference to determine the enhancement factor. The enhancement factor is determined by taking the magnitude of the emission peak above the background and dividing by the free-film emission at the same wavelength. The enhancement factors for E_x1, E_y1, E_y2, and E_y3 are shown in Fig. 7. The data shown are composed of measurements performed on different samples using both P3HT and PS polymers. Note that the expected linear dependence of the enhancement factor on Q due to the Purcell effect is absent, confirming that PbS belongs to the "bad emitter" class. The exact value of the homogeneous linewidth of PbS is still under debate [35,51–53]. From single QD measurements of PbS emitting at 800 nm [52] and temperature-dependent measurements of PbS emission at

Table 2. Estimated Enhanced Emission Factor Referenced to Free-Film

	Q	A (Excitation Spot Area)	EF_A	EF_D	$\mathrm{EF}_{\mathrm{cav}}$	Coupling of QD Emission to Microcavity	Coupling of the Emission to Free Space	Collection Efficiency	Signal Strength (au)	Estimated	Measured Ratio (Normalized Area)
Free-film (.65NA)		1.00	1.00	1.80	n/a	n/a	1.00	0.42	0.8	1	1
$1.0W_1$ resonances	100	0.16	1.30	7.30	2	0.32	1.00	1.00	4.7	6	30
E_x1 resonance	500	0.16	1.30	7.30	3	0.32	1.00	1.00	9.1	12	75
E_y3 resonance	2000	0.16	1.30	7.30	3	0.32	1.00	1.00	9.1	12	75

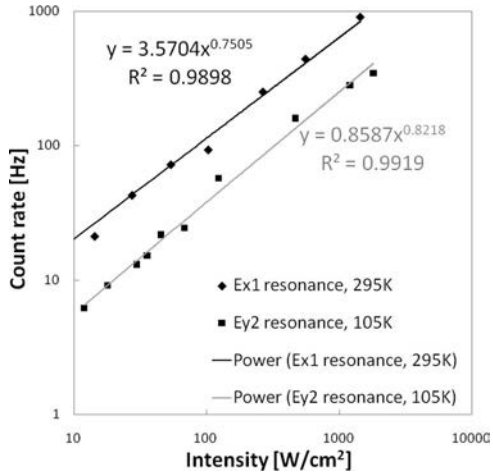

Fig. 8. Intensity dependent yield of E_x1 resonance at 295 K (diamonds) and E_y2 resonance at 105 K (squares), along with the power dependence fit to $y = ax^b$. The fit parameters and quality of fit are shown in the figure.

1100 nm [53], the homogeneous width was determined to be 90–100 meV. This linewidth is significantly larger than the dephasing width of 1.2 meV measured by pump–probe experiments in solution [35], a value consistent with the relationship between the absorption cross section and the radiative lifetime. The dephasing width is known to increase significantly when QDs are cast in solid film form [22]. Our own independent measurement confirms that the luminescence yield decreases by a factor of 10 when the quantum suspension film coalesces into a close-packed monolayer film on a water surface, resulting in a 12 meV homogeneous linewidth. Even using this optimistic homogeneous width, we find the Purcell enhancement effect saturates at a value of 3.

As discussed in Subsection 3.C, the dielectric enhancement including the local field effect is approximately 7.3. Again, as in the waveguide mode case, we assume a maximum value of 1 for the β coupling factor, η_{FS} free-space coupling efficiency, and η_C collection efficiency, yet the estimated emission strength is still a factor of 6 less than our observation.

A remaining concern is whether the observed emission enhancement is actually from amplified spontaneous emission. To address this question, we performed intensity-dependent studies and found three pieces of evidence to preclude this effect. First, with a change in excitation intensity from 10 to 10^4 W/cm^2, we did not find an increase in slope in the emission intensity versus excitation intensity, which would indicate a transition from spontaneous emission to amplified spontaneous emission (Fig. 8). In fact, they all show sublinear behavior, which fits very well to a power law dependence of the form $y = ax^b$, with $b = 0.75$ for the E_x1 resonance at room temperature and $b = 0.82$ for the E_y2 resonance at 105 K. This sublinear behavior [54] is commonly observed in colloidal QD PL and is believed to be associated with quenching processes [55]. Second, the ratio between each emission peak and the background remains constant to within <20% over the same 3 orders of magnitude change in excitation intensities, indicating that there is no spectral redistribution upon change in pump intensity. Third, we observed neither linewidth narrowing nor any broadening for E_x1, E_y2, and E_y3 resonances with changes to pump power.

4. DISCUSSION AND CONCLUSION

We observed an approximate 75-fold enhancement in the emission from microcavity resonances and a 30-fold enhancement from FP-like waveguide modes. The lack of a linear relationship between the enhancement factor and cavity Q, and the fact that PbS QDs are "bad emitters," indicate that the Purcell effect is not expected to be the dominant enhancement mechanism. After including the local field dielectric enhancement, the observed enhancement factor is still 5–6 times larger than expected. We believe the actual discrepancy is higher since we made generous estimates on the angular redistribution and collection efficiency. We are also able to rule out enhanced absorption based on the relative emission strength from the cavity-free patterned region and free-film using FDTD numerical simulations. Intensity dependent measurements of the emission and linewidth also exclude amplified spontaneous emission. Conclusive confirmation of this enhancement factor requires lifetime measurements of emitters in these structures, and presently, this measurement is not feasible. Nevertheless, the spectral energy content of the QD emission that couples to the FP-like resonance is 85% of the total emission from a free-film. This is very significant because it shows that one can reshape the broad emission spectrum in a very efficient way.

Using Fermi's golden rule, saturation of the Purcell enhancement factor is based on the notion that the oscillator strength of the dipole is spread out over a large bandwidth and, therefore, the benefit of the high cavity Q and small volume can only impact this narrow portion of the homogeneous linewidth. However, this analysis does not take into consideration QD–QD interactions and interactions with the thermal bath. In the experiments reported here, the QDs in these close-packed films are separated from each other by a 1–2 nm gap, which means that they are far from independent emitters. It is expected that these interactions cannot be ignored.

Anomalous enhancement in emission was also observed from Rhodamine 6G coupled to morphology-dependent optical modes in liquid droplets [56]. The enhancement mechanism was interpreted as interaction of the excited molecule with surrounding solvent molecules causing the emission wavelength to wander dynamically, a phenomenon called spectral diffusion [57]. The time it takes to wander through the homogeneous linewidth of Rhodamine is estimated to be comparable to its radiative lifetime of 3.6 ns. The spectral diffusion effect is also prevalent in QD systems. Subnanosecond spectral diffusion time in a CdSe QD system was recently reported [58]. This mechanism can effectively enlarge the spectral bandwidth that can contribute to the cavity emission; therefore, this mechanism is likely to contribute significantly an additional enhancement in emission in our experiment within a much longer radiative lifetime of 2 μs.

Dipole–dipole interaction (Förster process) between excited–excited and excited–unexcited QDs is also expected to be strong due to their close proximity. Evidence of this process in a PbS quantum system was also reported [59]. This mechanism can also cause excitons in the excited region to spread beyond the excitation region unless there is a mechanism to cause the donors to preferentially give their energy to acceptors inside the cavity. The cavity-enhanced Förster process has been reported in planar cavity geometries [60,61]. However, this effect [62,63] is much smaller than the observed

enhancement effect in [60]. Since the typical time scale for Förster processes is of the order of nanoseconds, this is not expected to be as important as spectral diffusion.

Recently, phonon interaction has been shown to be important in coupling off-resonant QD excitation to emit at the cavity resonant frequency [64]. Majumdar *et al.* in [64] introduce phonon interaction to a two-level system coupled to an optical cavity and have shown significant enhanced emission at the cavity frequency due to several orders of magnitude increase in off-resonant coupling. This coupling mechanism allows nonresonant QDs to emit at the cavity wavelength and hence can increase the cavity emission beyond what Fermi's golden rule can account for. The basic requirement for this mechanism to work is the presence of a dephasing mechanism. For the PbS system, the dephasing time is about 300 fs in film form based on the 12 meV linewidth we discussed. Because this coupling mechanism is not sensitive to the coupling strength between emitter and cavity, in other words, valid for both the strong and weak coupling regimes, this effect is expected to be present in our experiment and can provide an additional enhancement in emission [65].

In summary, the anomalous enhanced emission we observed may be due to spectral diffusion mediated by induced polarization of the environment and phonons, which enable a larger part of the homogeneous and inhomogeneous emitter linewidths to contribute to the cavity emissions. More experimental studies are planned to investigate these effects by controlling the particle spacing and temperature.

ACKNOWLEDGMENTS

The authors acknowledge fruitful discussions with Alon Gabbay, R. Kekatpure, and Mike Sinclair, numerical simulations from I. El-Kady, M. M. Su, B. G. Farfan, and M. R. Taha, and fabrication support from the staff at the Microelectronics Development Laboratory (MDL) at Sandia National Laboratories (SNL). Support for this work is from SNL's Laboratory Directed Research Development (LDRD) program and by the U.S. Department of Energy (DOE) through the Office of Science, Office of Basic Energy Sciences (BES) for manuscript preparation and Energy Frontier Research Center (EFRC) for Solid-State Lighting Science for data analysis and Center for Integrated Nanotechnologies (CINT, national user facility) for experimental activities. SNL is a multiprogram laboratory operated by Sandia Corporation, a part of Lockheed-Martin Corporation, for the U.S. DOE under Contract No. DE-AC04-94AL85000.

REFERENCES

1. K. J. Vahala, "Optical microcavities," Nature **424**, 839–846 (2003).
2. J. Wiersig, C. Gies, F. Jahnke, M. Aszmann, T. Berstermann, M. Bayer, C. Kistner, S. Reitzenstein, C. Schneider, S. Hofling, A. Forchel, C. Kruse, J. Kalden, and D. Hommel, "Direct observation of correlations between individual photon emission events of a microcavity laser," Nature **460**, 245–249 (2009).
3. M. Pelton, C. Santori, J. Vuckovic, B. Zhang, G. S. Solomon, J. Plant, and Y. Yamamoto, "Efficient source of single photons: a single quantum dot in a micropost microcavity," Phys. Rev. Lett. **89**, 233602 (2002).
4. C. Santori, D. Fattal, J. Vuckovic, G. S. Solomon, and Y. Yamamoto, "Indistinguishable photons from a single-photon device," Nature **419**, 594–597 (2002).
5. B. Lounis and M. Orrit, "Single-photon sources," Rep. Prog. Phys. **68**, 1129–1179 (2005).
6. G. Khitrova, H. M. Gibbs, M. Kira, S. W. Koch, and A. Scherer, "Vacuum Rabi splitting in semiconductors," Nat. Phys. **2**, 81–90 (2006).
7. A. J. Shields, "Semiconductor quantum light sources," Nat. Photon. **1**, 215–223 (2007).
8. P. Michler, A. Imamoglu, M. D. Mason, P. J. Carson, G. F. Strouse, and S. K. Buratto, "Quantum correlation among photons from a single quantum dot at room temperature," Nature **406**, 968–970 (2000).
9. M. Boroditsky, R. Vrijen, T. F. Krauss, R. Coccioli, R. Bhat, and E. Yablonovitch, "Spontaneous emission extraction and Purcell enhancement from thin-film 2-D photonic crystals," J. Lightwave Technol. **17**, 2096–2112 (1999).
10. T. Tanabe, K. Nishiguchi, E. Kuramochi, and M. Notomi, "Low power and fast electro-optic silicon modulator with lateral p-i-n embedded photonic crystal nanocavity," Opt. Express **17**, 22505–22513 (2009).
11. J. M. Phillips, P. E. Burrows, R. F. Daves, J. A. Simmons, G. G. Malliaras, F. So, J. A. Misewich, A. V. Nurmikko, and D. L. Smith, "Basic research needs for solid-state lighting," Basic Energy Sciences report (U.S. Department of Energy, 2006), http://www.sc.doe.gov/bes/reports/files/SSL_rpt.pdf.
12. M. Ji, S. Park, S. T. Connor, T. Mokari, Y. Cui, and K. J. Gaffney, "Efficient multiple exciton generation observed in colloidal PbSe quantum dots with temporally and spectrally resolved intraband excitation," Nano Lett. **9**, 1217–1222 (2009).
13. T. Tiedje, E. Yablonovitch, G. D. Cody, and B. G. Brooks, "Limiting efficiency of silicon solar cells," IEEE Trans. Electron Devices **ED-31**, 711–716 (1984).
14. A. Kress, F. Hofbauer, N. Reinelt, M. Kaniber, H. J. Krenner, R. Meyer, G. Bohm, and J. J. Finley, "Manipulation of the spontaneous emission dynamics of quantum dots in two-dimensional photonic crystals," Phys. Rev. B **71**, 241304(R) (2005).
15. T. Lund-Hansen, S. Stobbe, B. Julsgaard, H. Thyrrestrup, T. Sunner, M. Kamp, A. Forchel, and P. Lodahl, "Experimental realization of highly efficient broadband coupling of single quantum dots to a photonic crystal waveguide," Phys. Rev. Lett. **101**, 113903 (2008).
16. M. Makarova, J. Vuckovic, H. Sanda, and Y. Nishi, "Silicon-based photonic crystal nanocavity light emitters," Appl. Phys. Lett. **89**, 221101 (2006).
17. M. Nomura, N. Kumagai, S. Iwamoto, Y. Ota, and Y. Arakawa, "Photonic crystal nanocavity laser with a single quantum dot gain," Opt. Express **17**, 15975–15982 (2009).
18. I. Fushman, D. Englund, A. Faraon, N. Stoltz, P. Petroff, and J. Vuckovic, "Controlled phase shifts with a single quantum dot," Science **320**, 769–772 (2008).
19. A. Faraon, I. Fushman, D. Englund, N. Stoltz, P. Petroff, and J. Vuckovic, "Coherent generation of non-classical light on a chip via photon-induced tunnelling and blockade," Nature Phys. **4**, 859–863 (2008).
20. I. Fushman, D. Englund, and J. Vuckovic, "Coupling of PbS quantum dots to photonic crystal cavities at room temperature," Appl. Phys. Lett. **87**, 241102 (2005).
21. M. Fujita, Y. Tanaka, and S. Noda, "Light emission from silicon in photonic crystal nanocavity," IEEE J. Sel. Top. Quantum Electron. **14**, 1090–1097 (2008).
22. Z. Wu, Z. Mi, P. Bhattacharya, T. Zhu, and J. Xu, "Enhanced spontaneous emission at 1.55 μm from colloidal PbSe quantum dots in a Si photonic crystal microcavity," Appl. Phys. Lett. **90**, 171105 (2007).
23. M. Makarova, V. Sih, J. Warga, R. Li, L. Dal Negro, and J. Vuckovic, "Enhanced light emission in photonic crystal nanocavities with erbium-doped silicon nanocrystals," Appl. Phys. Lett. **92**, 161107 (2008).
24. A. G. Pattantyus-Abraham, H. Qiao, J. Shan, K. A. Abel, T.-S. Wang, F. C. J. M. van Veggel, and J. F. Young, "Site-selective optical coupling of PbSe nanocrystals to Si-based photonic crystal microcavities," Nano Lett. **9**, 2849–2854 (2009).
25. J. Yang, J. Heo, T. Zhu, J. Xu, J. Topolancik, F. Vollmer, R. Ilic, and P. Bhattacharya, "Enhanced photoluminescence from embedded PbSe colloidal quantum dots in silicon-based random photonic crystal microcavities," Appl. Phys. Lett. **92**, 261110 (2008).
26. Y. Gong, M. Makarova, S. Yerci, R. Li, M. J. Stevens, B. Baek, S. W. Nam, R. H. Hadfield, S. N. Dorenbos, V. Zwiller, J. Vuckovic,

and L. Dal Negro, "Linewidth narrowing and Purcell enhancement in photonic crystal cavitieson an Er-doped silicon nitride platform," Opt. Express **18**, 2601–2612 (2010).
27. A. Meldrum, P. Bianucci, and F. Marsiglio, "Modification of ensemble emission rates and luminescence spectra for inhomogeneously broadened distributions of quantum dots coupled to optical microcavities," Opt. Express **18**, 10230–10246 (2010).
28. H. Y. Ryu and M. Notomi, "Enhancement of spontaneous emission from the resonant modes of a photonic crystal slab single-defect cavity," Opt. Lett. **28**, 2390–2392 (2003).
29. Y. Xu, R. K. Lee, and A. Yariv, "Finite-difference time-domain analysis of spontaneous emission in a microdisk cavity," Phys. Rev. A **61**, 033808 (2000).
30. M. Makarova, V. Sih, J. Warga, R. Li, L. Dal Negro, and J. Vuckovic, "Enhanced light emission in photonic crystal nanocavities with erbium-doped silicon nanocrystals," Appl. Phys. Lett. **92**, 161107 (2008).
31. S. Xiong, X. Miao, J. Spencer, C. Khripin, T. S. Luk, and C. J. Brinker, "Integration of a close-packed quantum dot monolayer with a photonic-crystal cavity via interfacial self-assembly and transfer," Small **6**, 2126–2129 (2010).
32. Y. Akahane, T. Asano, B. S. Song, and S. Noda, "High-Q photonic nanocavity in a two-dimensional photonic crystal," Nature **425** (2003).
33. J. Pang, S. Xiong, F. Jaeckel, Z. Sun, D. Dunphy, and C. J. Brinker, "Free-standing, patternable nanoparticle/polymer monolayer arrays formed by evaporation induced self-assembly at a fluid interface," J. Am. Chem. Soc. **130**, 3284–3285 (2008).
34. H. Fan, K. Yang, D. M. Boye, T. Sigmon, K. J. Malloy, H. Xu, G. P. López, and C. J. Brinker, "Self-assembly of ordered, robust, three-dimensional gold nanocrystal/silica arrays," Science **304**, 567–571 (2004).
35. R. D. Schaller, J. M. Pietryga, S. V. Goupalov, M. A. Petruska, S. A. Ivanov, and V. I. Klimov, "Breaking the phonon bottleneck in semiconductor nanocrystals via multiphonon emission induced by intrinsic nonadiabatic interactions," Phys. Rev. Lett. **95**, 196401 (2005).
36. J. M. An, M. Califano, A. Franceschetti, and A. Zunger, "Excited-state relaxation in PbSe quantum dots," J. Chem. Phys. **128**, 164720 (2008).
37. J. D. Joannopoulos, S. G. Johnson, J. N. Winn, and R. D. Meade, *Photonic Crystals Molding the Flow of Light* (Princeton Univ. Press, 2008).
38. V. A. Mandelshtam and H. S. Taylor, "Harmonic inversion of time signals and its applications," J. Chem. Phys. **107**, 6756–6769 (1997).
39. N.-V.-Q. Tran, S. Combrie, and A. De Rossi, "Directive emission from high-*Q* photonic crystal cavities through band folding," Phys. Rev. B **79**, 041101 (2009).
40. J.-Y. Zhang, X.-Y. Wang, and M. Xiao, "Modification of spontaneous emission from CdSe/CdS quantum dots in the presence of a semiconductor interface," Opt. Lett. **27**, 1253–1255 (2002).
41. M. E. Crenshaw, "The quantized field in a dielectric and application to the radiative decay of an embedded atom," Phys. Lett. A **358**, 438–442 (2006).
42. K. Dolgaleva, R. W. Boyd, and P. W. Milonni, "Influence of local-field effects on the radiative lifetime of liquid suspensions of Nd:YAG nanoparticles," J. Opt. Soc. Am. B **24**, 516–521 (2007).
43. P. R. Berman and P. W. Milonni, "Microscopic theory of modified spontaneous emission in a dielectric," Phys. Rev. Lett. **92**, 053601 (2004).
44. R. J. Glauber and M. Lewenstein, "Quantum optics of dielectric media," Phys. Rev. A **43**, 467–491 (1991).
45. H. A. Lorentz, *Theory of Electrons and Its Applications to the Phenomena of Light and Radiant Heat* (Stechert, 1916).
46. M. E. Crenshaw and C. M. Bowden, "Effects of local fields on spontaneous emission in dielectric media," Phys. Rev. Lett. **85**, 1851–1854 (2000).
47. E. He, H. Zheng, X. Zhang, and S. Qu, "Local-field effect on the fluorescence relaxation of Tm3 + :LaF3 nanocrystals immersed in liquid medium," Luminescence **25**, 66–70 (2010).
48. N. Ganesh, W. Zhang, P. C. Mathias, E. Chow, J. A. N. T. Soares, V. Malyarchuk, A. D. Smith, and B. T. Cunningham, "Enhanced fluorescence emission from quantum dots on a photonic crystal surface," Nat. Nanotechnol. **2**, 515–520 (2007).
49. J.-K. Hwang, H.-Y. Ryu, and Y.-H. Lee, "Spontaneous emission rate of an electric dipole in a general microcavity," Phys. Rev. B **60**, 4688–4695 (1999).
50. S. Fan, P. R. Villeneuve, J. D. Joannopoulos, and E. F. Schubert, "High extraction efficiency of spontaneous emission from slabs of photonic crystals," Phys. Rev. Lett. **78**, 3294–3297 (1997).
51. J. M. Harbold and F. W. Wise, "Photoluminescence spectroscopy of PbSe nanocrystals," Phys. Rev. B **76**, 125304 (2007).
52. J. J. Peterson and T. D. Krauss, "Fluorescence spectroscopy of single lead sulfide quantum dots," Nano Lett. **6**, 510–514 (2006).
53. L. Turyanska, A. Patane, M. Henini, B. Hennequin, and N. R. Thomas, "Temperature dependence of the photoluminescence emission from thiol-capped PbS quantum dots," Appl. Phys. Lett. **90**, 101913 (2007).
54. V. I. Klimov, A. A. Mikhailovsky, S. Xu, A. Malko, J. A. Hollingsworth, C. A. Leatherdale, H. J. Eisler, and M. G. Bawendi, "Optical gain and stimulated emission in nanocrystal quantum dots," Science **290**, 314–317 (2000).
55. S. Liao, M. Dutta, D. Schonfeld, T. Yamanaka, and M. Stroscio, "Quantum dot blinking: relevance to physical limits for nanoscale optoelectronic device," J. Comput. Electron. **7**, 462–465 (2008).
56. M. D. Barnes, W. B. Whitten, and J. M. Ramsey, "Enhanced fluorescence yields through cavity quantum-electrodynamic effects in microdroplets," J. Opt. Soc. Am. B **11**, 1297–1304 (1994).
57. A. D. Stein and M. D. Fayer, "Spectral diffusion in liquids," J. Chem. Phys. **97**, 2948–2962 (1992).
58. G. Sallen, A. Tribu, T. Aichele, R. Andre, L. Besombes, C. Bougerol, M. Richard, S. Tatarenko, K. Kheng, and J. P. Poizat, "Subnanosecond spectral diffusion measurement using photon correlation," Nat. Photon. **4**, 696–699 (2010).
59. S. W. Clark, J. M. Harbold, and F. W. Wise, "Resonant energy transfer in PbS quantum dots," J. Phys. Chem. C **111**, 7302–7305 (2007).
60. P. Andrew and W. L. Barnes, "Förster energy transfer in an optical microcavity," Science **290**, 785–788 (2000).
61. C. E. Finlayson, D. S. Ginger, and N. C. Greenham, "Enhanced Forster energy transfer in organic/inorganic bilayer optical microcavities," Chem. Phys. Lett. **338**, 83–87 (2001).
62. G. S. Agarwal and S. D. Gupta, "Microcavity-induced modification of the dipole-dipole interaction," Phys. Rev. A **57**, 667–670 (1998).
63. T. Kobayashi, Q. Zheng, and T. Sekiguchi, "Resonant dipole-dipole interaction in a cavity," Phys. Rev. A **52**, 2835–2846 (1995).
64. A. Majundar, Y. Y. Gong, E. D. Kim, and J. Vuckovic, "Phonon mediated off-resonant quantum dot-cavity coupling," arXiv:1012.3125v1 (2010).
65. S. Ates, S. M. Ulrich, A. Ulhaq, S. Reitzenstein, A. Loffler, S. Hofling, A. Forchel, and P. Michler, "Non-resonant dot-cavity coupling and its potential for resonant single-quantum-dot spectroscopy," Nat. Photon. **3**, 724–728 (2009).